Electronic Supplementary Information (ESI)

Self-Assembled Organic Homostructures with Tunable Emission, Multi-Directional Waveguide and Identical Crystal Parameters Fabricated via "Cocrystal Engineering"

Ying Xin Ma, Guo Qing Wei, Song Chen, Hong Tao Lin and Xue Dong Wang**

Y. X. Ma, G. Q. Wei, S. Chen, Dr. H. T. Lin, Prof. X. D. Wang

School of Chemistry and Chemical Engineering, Shandong University of Technology, Zibo, Shandong 255000, P. R. China.
E-mail: linht@sdut.edu.cn (H. T. Lin)
Institute of Functional Nano & Soft Materials (FUNSOM), Jiangsu Key Laboratory for Carbon-Based Functional Materials & Devices, Soochow University, 199 Ren'ai Road, Suzhou, Jiangsu 215123, P. R. China
E-mail: wangxuedong@suda.edu.cn (X. D. Wang)

Experimental details

1. Materials

Organic compound tetratertbutylperylene (TBPe), 2,4,5,6-tetrachloroisophthalonitrile (*o*-TCP), 3,4,5,6-tetrachloroisophthalonitrile (*m*-TCP) and 2,3,5,6-tetrachloroterephthalonitrile (*p*-TCP) was purchased from Shanghai Dibai Biological Technology Inc., and used without further purification.

2. Preparation of TBPe-TCP cocrystals

The TBPe-TCP cocrystals were prepared by the facile solution-drying method. For the cocrystals with rod-like morphology, 46 mg TBPe and 27 mg *o*-TCP, *m*-TCP and *p*-TCP powder were mixed with 5 ml acetonitrile in four test tubes respectively. The cocrystal of TBPe with *o*-TCP (CC-A) can be prepared by mixing 0.2 ml corresponding precursors and dropping onto the glass slide for solvent evaporation. The rod-like cocrystals of TBPe with *m*-TCP (CC-B) and *p*-TCP (CC-C) can be prepared by the same process.

For the cocrystals with branched morphology, 46 mg TBPe and 27 mg *o*-TCP, *m*-TCP and *p*-TCP powder were mixed with 5 ml acetonitrile in four test tubes respectively. The cocrystal of TBPe with *o*-TCP (CC-A) can be prepared by mixing 0.2 ml corresponding precursors, adding 0.4 ml dichloromethane and then dropping the obtained solution onto the glass slide for solvent evaporation. The branched cocrystals of TBPe with *m*-TCP (CC-B) and *p*-TCP (CC-C) can be prepared by the same process.

3. Optical Characterizations

The steady-state fluorescence spectra of the samples were measured by a HITACHI F-4600 fluorescence spectrophotometer. Meanwhile, the time-resolved femtosecond fluorescence up-conversion measurement were performed using a Pharos femtosecond laser system (Light Conversion; 1030 nm, 250 fs, 200 uJ/pulse and 100 kHz repetition frequency) and a HARPIA-TF up-conversion system incorporated with TCSPC module. The fluorescence microscopy images were obtained using a Leica DMRBE fluorescence microscope with a spot-enhanced charge couple device (CCD, Diagnostic Instrument, Inc.). TEM images were obtained by a transmission electron microscopy (TEM, FEI company, Tecnai G2 F20, United States). One drop of the solution was dropped on a carbon-coated copper grid, and evaporated at room temperature. TEM measurement was performed at an accelerating voltage of 20 kV. Micro-area photoluminescence (μ-PL) spectra were collected on a homemade optical microscopy and the equipment were set up as shown in the Scheme S1. The light was coupled to a grating spectrometer (Princeton Instrument, ARC-SP-2356) and recorded by a thermal-electrically cooled CCD (Princeton Instruments, PIX-256E). PL microscopy images were taken with an inverted microscope (Olympus, BX43). The single crystal XRD data were collected at 120 K on a Bruker SMART APEX II, Mo $K\alpha$ (λ = 0.71073 Å). The data were processed with Denzoscalepack. Solution and refinement: Structures were solved by direct methods with SHELXS. Full matrix least-squares refinement on the basis of F^2 with SHELXS-97. Refinement of F^2 was against all reflections. Stacking distances were determined by calculating the best plane through a ring and subsequent

determination of the distance of the ring atoms of the neighboring molecule and averaging of these distances.

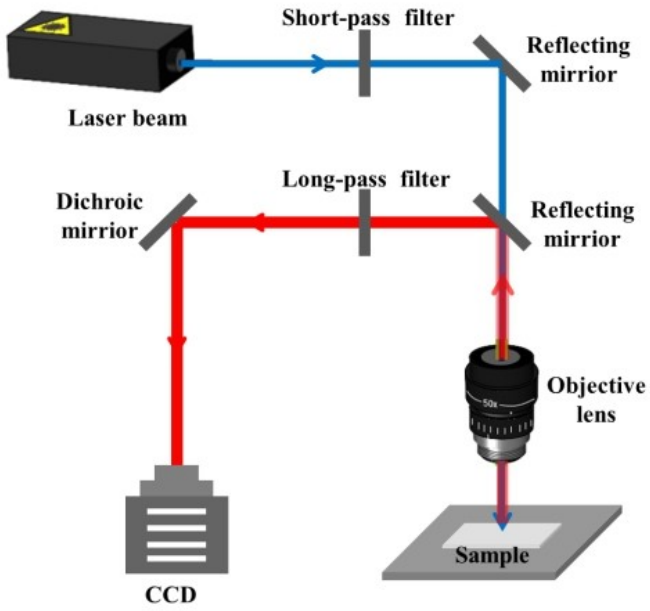

Figure S1. Schematic demonstration of the experimental setup for the optical characterization.

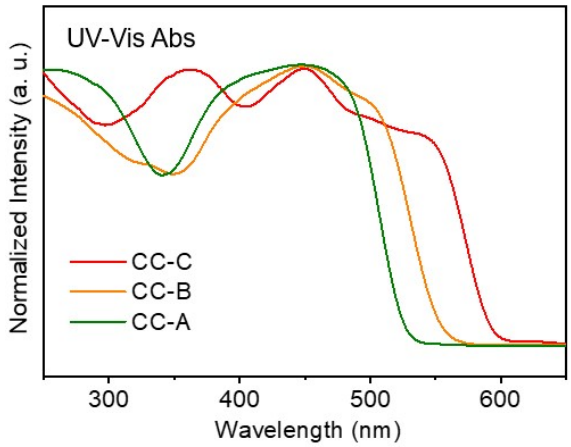

Figure S2. UV-Vis absorption spectra of CC-A, CC-B and CC-C.

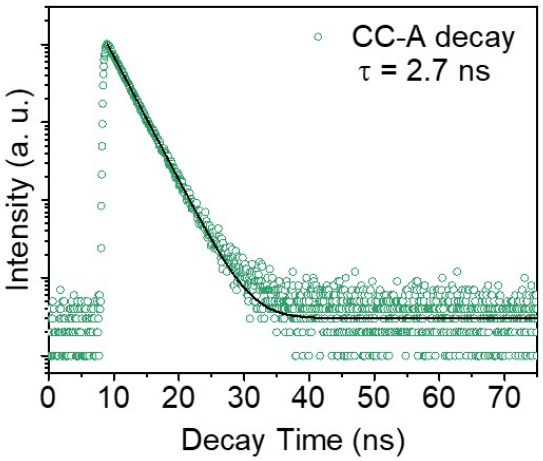

Figure S3. The PL lifetime decay and fitted curve for CC-A.

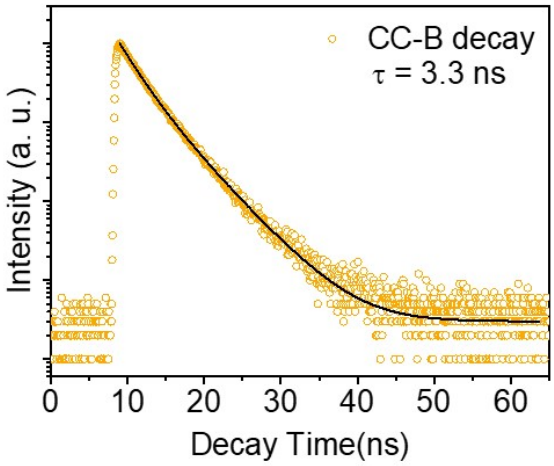

Figure S4. The PL lifetime decay and fitted curve for CC-B.

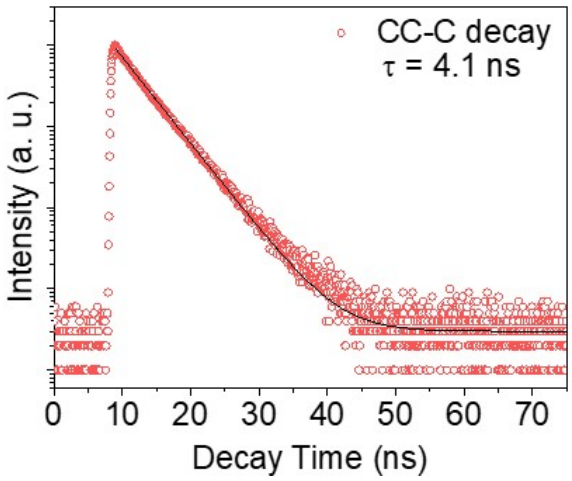

Figure S5. The PL lifetime decay and fitted curve for CC-C.

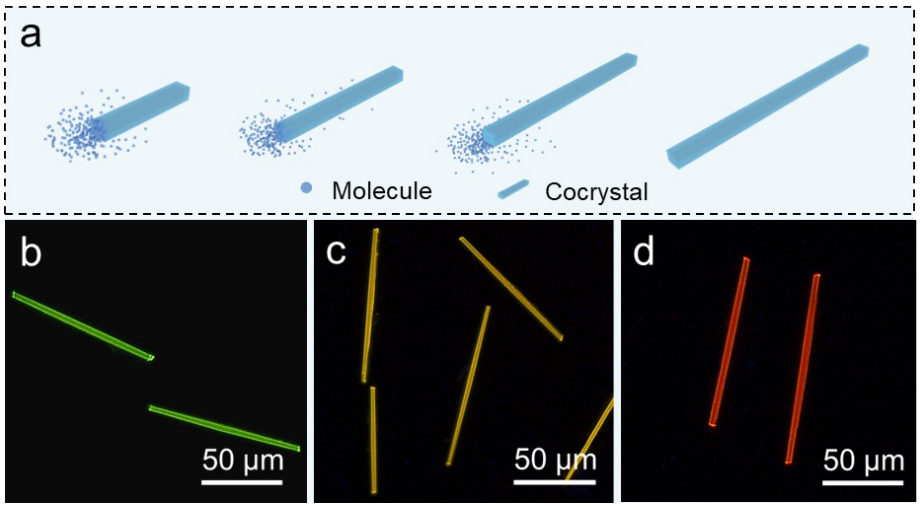

Figure S6. a) Schematic illustration of the rod-like cocrystal growth process. b-d) The PL images of the cocrystals CC-A, CC-B and CC-C with rod-like morphology.

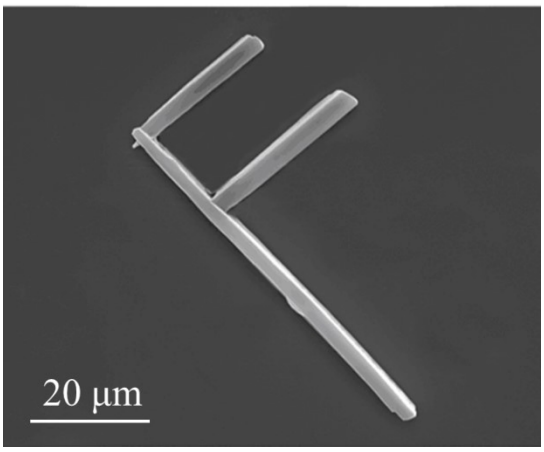

Figure S7. SEM image of an individual branched CC-C.

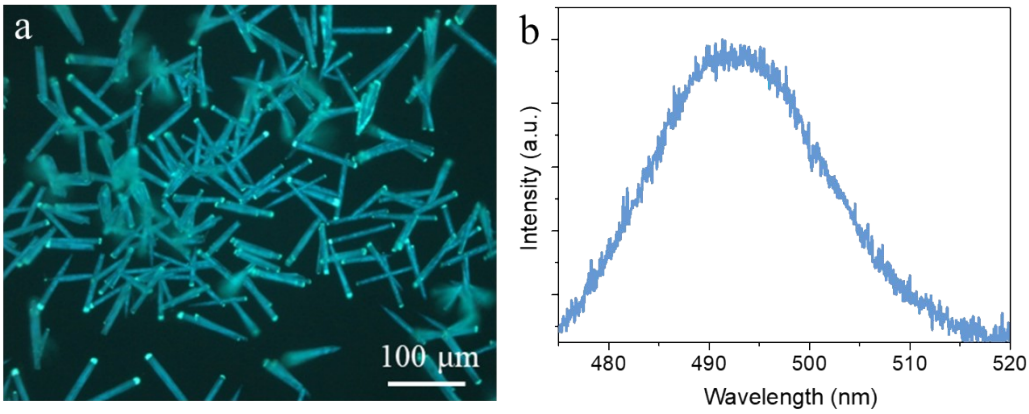

Figure S8. a) PL images of TBPe micro single crystals. b) PL spectrum of TBPe micro single crystals.

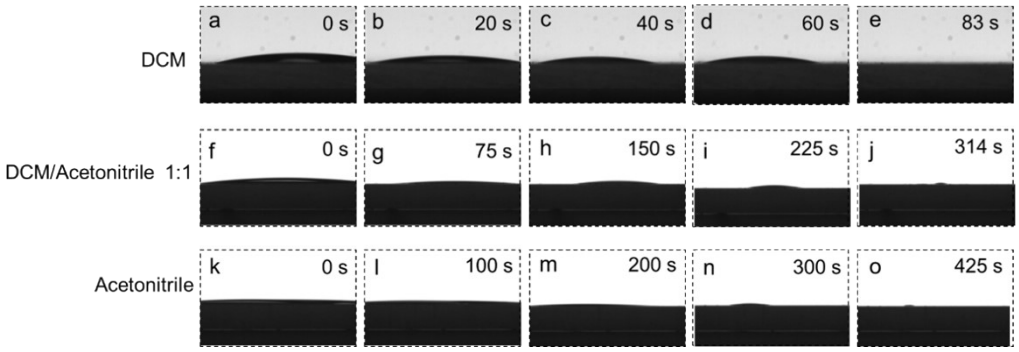

Figure S9. a-e) The images showing the evaporation process of dichloromethane after 0s, 20s, 40s, 60s and 83s respectively. f-j) The images showing the evaporation process of the 1:1 mixed dichloromethane and acetonitrile solvent after 0s, 75s, 150s, 225s and 314s respectively. k-o) The images showing the evaporation process of acetonitrile after 0s, 100s, 200s, 300s and 425s respectively.

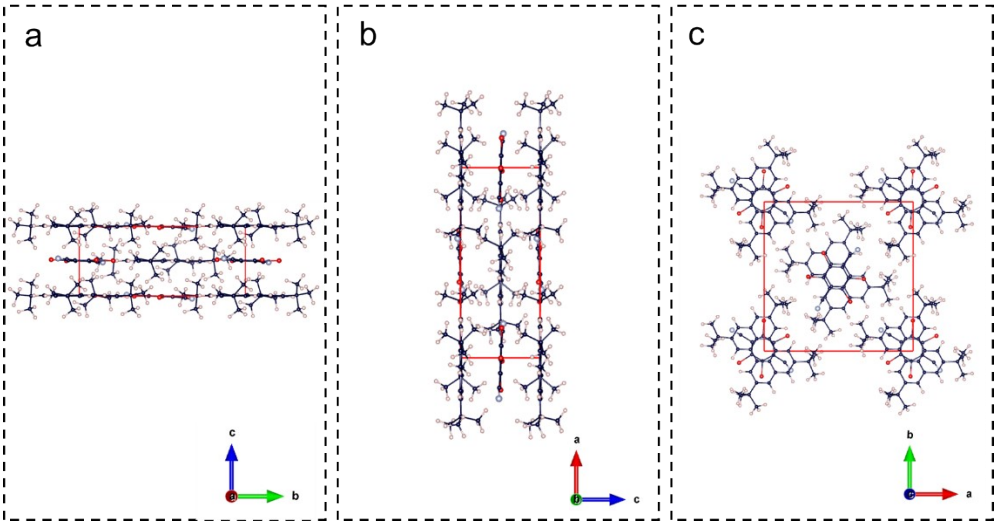

Figure S10. Schematic showing the molecular packing mode of CC-C from a) a, b) b and c) c axis views.

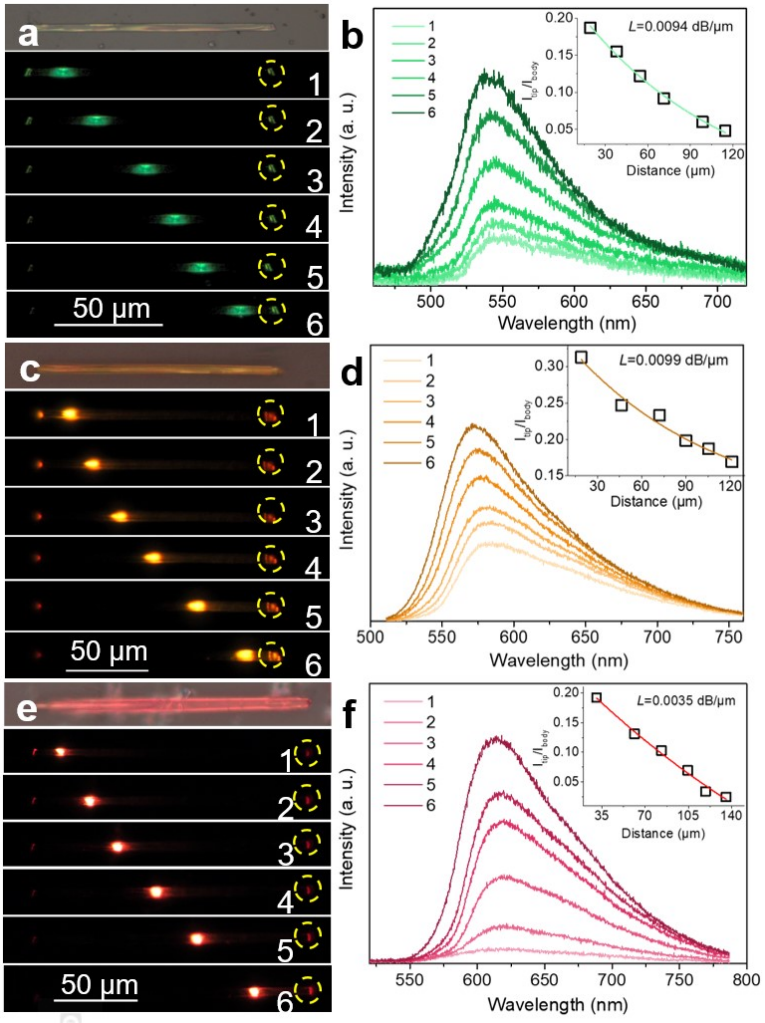

Figure S11. (a, c, e) The bright filed and PL images of rod-like CC-A, CC-B, CC-C with the 375 nm excitation spot moving from the left to right terminal; (b, d, f) The PL spectra at the corresponding right terminal labeled with numbers 1-6 in a, c, e respectively.

The rod-like cocrystals of CC-A, CC-B and CC-C exhibit superior optical waveguide performance with very low loss coefficient *L*. As shown in Fig. S11a, c and e, the waveguide performance of these cocrystal rods is investigated by the home-made micro area optical measurement system (Fig. S1). The 375 nm UV beam is focused on the rods for excitation and moved from the left terminal to the right sequentially, the PL

spectra at the right ends on the rods are taken for further analysis (labelled with numbers 1-6). Fig. S11b, d and f show the corresponding PL spectra collected from the rods of CC-A, CC-B and CC-C respectively. The results show that the terminal PL spectra intensity rise gradually with the excitation spot moving close to the right terminal of the rods. The insets demonstrate the relationship of I_{tip}/I_{body} and the distance from the excitation spot to the right tip D, where I_{tip} is the PL intensity of the right tip, and I_{body} is the PL intensity at the corresponding excitation spot. The optical loss coefficient L can be obtained by the decay fitting:

$$I_{tip}/I_{body} = Aexp(-LD)$$

The fitted curves are shown in the insets of Figure S11b, d and f. The values of L for CC-A, CC-B and CC-C are as low as 0.0094 dB/μm, 0.0099 dB/μm and 0.0035 dB/μm respectively, which suggests the extraordinary optical waveguide performance of these rod cocrystals.

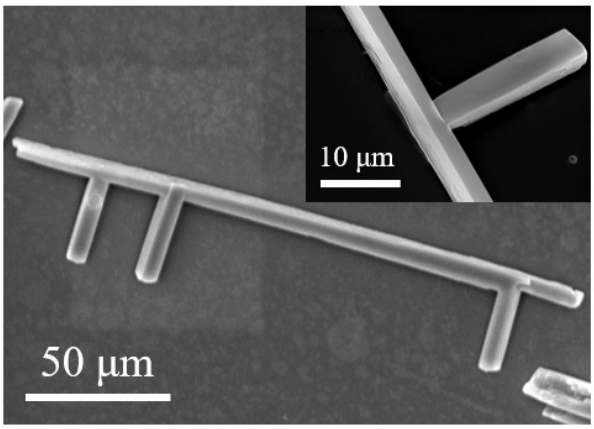

Figure S12. SEM image of a typical CC-C branched cocrystal with the scale bar of 50 μm. Inset: the partial enlarged view with the scale bar of 10 μm.

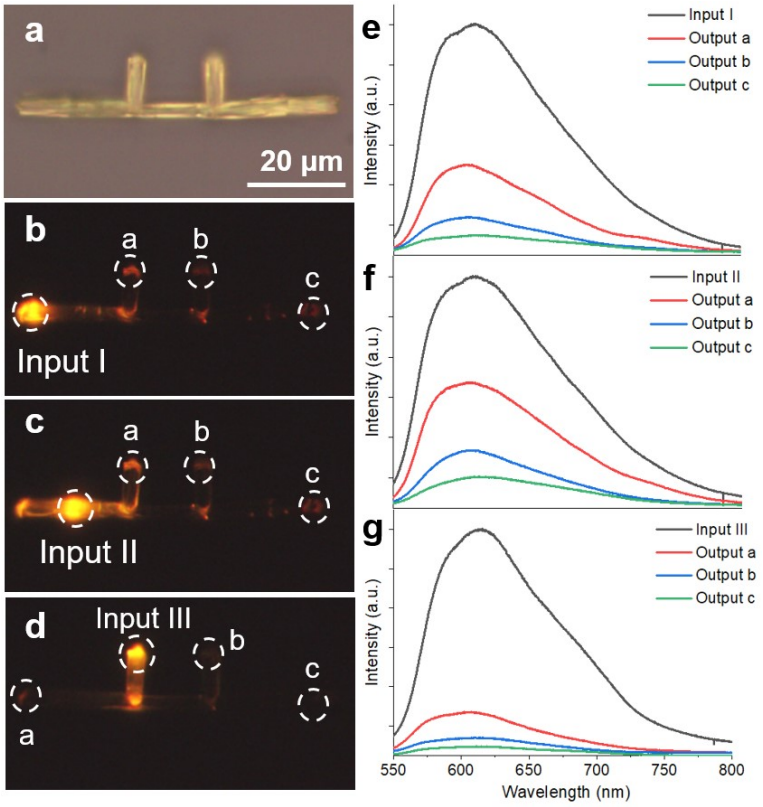

Figure S13. (a) The bright filed image of an individual branched CC-C; (b) The PL image of the CC-C with 375 nm excitation laser focused at input I; (c) The PL image of the CC-C with 375 nm excitation laser focused at input II; (d) The PL image of the CC-C with 375 nm excitation laser focused at input III; (e-g) The corresponding PL spectra at the input terminal and output terminals a-c for Fig. S12b-d respectively.

In order to better explain the optical properties of the isomorphous crystals, a single branched CC-C cocrystal homostructure is selected under the micro area optical measurement system to perform the optical waveguide investigation (Figure S12a). As shown in Figure S12b and 2c, the 375 nm laser beam is focused on the trunk and branch terminal of the cocrystal homostructure at different positions I, II and III as the input signal, and the PL spectra at the branch tips and the trunk terminal a, b, and c are taken for further analysis. The results are displayed in Figure S12e-g, which corresponds to

the PL spectra of the homostructures in Figure S12b-d respectively. For the situation shown in Figure S12c, the output PL intensity at a to c sequentially decreases as the horizontal distance (x axis direction) from the input position to output terminal increases. And when the excitation is performed at the extreme left side of the crystal terminal as Figure S12b shows, the output intensity at the branches will decrease compared with the excitation point in Figure S12c, which is due to the loss of the optical signal during propagate process, the longer the propagation distance is, the greater the loss of the optical signal will be until it reaches zero. Moreover, when the excitation is performed at the left side branch terminal, the output intensity at b and c is basically same, whereas the output intensity at a is higher than b and c. It can be summarized that the cocrystal homostructure can realize the diversion of photon flux during transportation.

Table S1. The unit cell parameters of the CC-A.

Cell constitution	TBPe-(*o*-TCP)
Crystal system	tetragonal
Space group	P 1
a (Å)	16.585
b (Å)	16.585
c (Å)	6.948
α (°)	90.000
β (°)	90.000
γ (°)	90.000
V (Å^3)	1911.114

Table S2. The unit cell parameters of the CC-B.

Cell constitution	TBPe-(*m*-TCP)
Crystal system	tetragonal
Space group	P 1
a (Å)	16.576
b (Å)	16.576
c (Å)	6.918
α (°)	90.000
β (°)	90.000
γ (°)	90.000
V (Å^3)	1900.802

Table S3. The unit cell parameters of the CC-C.

Cell constitution	TBPe-(*p*-TCP)
Crystal system	tetragonal
Space group	P 1
a (Å)	16.602
b (Å)	16.602
c (Å)	6.949
α (°)	90.000
β (°)	90.000
γ (°)	90.000
V (Å^3)	1915.328